MAUSAM, **77**, 1 (January 2025), 235-246

MAUSAM

DOI: https://doi.org/10.54302/9qqwq735
Homepage: https://mausamjournal.imd.gov.in/index.php/MAUSAM

UDC No. 551.574.42:551.509.3(594)

Assessment of frost events on the tropical highlands: Analyzing meteorological conditions and wrf-arw model performance on the Dieng plateau, Indonesia

ARIES KRISTIANTO[1]*, IMMA R. NUGRAHENI[1], RISTA H. VIRGIANTO[2,4], DENI SEPTIADI[1], HAPSORO A. NUGROHO[3,5], ITA SOEGIARTO[6], MAWAR J. FADHILAH[7], TRI WAHYUDI[8], RAVYDO A. JUFRI[9]

[1]*Department of Meteorology, State College of Meteorology, Climatology and Geophysics (STMKG), Tangerang, Indonesia*

[2]*Department of Climatology, State College of Meteorology, Climatology and Geophysics (STMKG), Tangerang, Indonesia*

[3]*Department of Instumentation, State College of Meteorology, Climatology and Geophysics (STMKG), Tangerang, Indonesia*

[4]*Department of Earth Sciences, University of Cambridge, United Kingdom CB2 3EQ*

[5]*Research Center for Artificial Intelligence and Data Engineering, Department of Electrical Engineering, Faculty of Engineering, Universitas Indonesia, Depok, Indonesia*

[6]*Rehabilitation Center, Ministry of Defense of the Republic of Indonesia, Jakarta, Indonesia*

[7]*Nabire Meteorological Station (BMKG),Papua, Indonesia*

[8]*Panjang Maritime Meteorological Station (BMKG), Bandar Lampung, Indonesia*

[9]*Gewanyantana Meteorological Station (BMKG), Larantuka, Flores Timur, Indonesia*

(*Received 10 October 2024, Accepted 15 April 2025*)

***Corresponding author's email: aries.kristianto@bmkg.go.id**

सार – डिएंग पठार (मध्य जावा, इंडोनेशिया) पर पाले का अध्ययन बाटुर AWS से प्राप्त 10-मिनट के प्रेक्षणों तथा WRF-ARW हिंडकास्ट का उपयोग करते हुए आठ घटनाओं (05-10 अगस्त; 01-02 सितंबर 2023) के लिए किया गया। निकट-सतह ऊष्मागतिकी का निदान ओसांक अवसाद ($\Delta = T - Td$) के माध्यम से किया गया और भौतिकी के दो विन्यासों का मूल्यांकन किया गया। अधिकांश रातों में वायु संतृप्ति के निकट पहुँच गई, जहाँ $\Delta min \leq$ लगभग 1-1.3 °C, सापेक्ष आर्द्रता ≈100% और सतही पवनें कमजोर (अक्सर $\leq$ 2 m s^{-1}) रहीं; न्यूनतम तापमान (Tmin) सामान्यतः Δmin के लगभग 70 मिनट बाद प्राप्त हुआ, जो दर्शाता है कि संतृप्ति के निकट पहुँचने के बाद भी शीतलन जारी रहता है।

एक घटना Δ के प्रतिरूप से भिन्न रही, जिससे संकेत मिलता है कि Δ अत्यधिक सूचनात्मक है, किंतु तब अनिवार्य नहीं रहता जब सूक्ष्म-स्तरीय सतही शीतलन, शेल्टर-स्तर की वायु से अलग हो। WRF ने दैनिक (डायर्नल) संरचना को पुनरुत्पादित किया, परंतु न्यूनतम तापमान के आसपास रात्रिकालीन व्यवस्थित उष्ण पूर्वाग्रह प्रदर्शित किया, जिससे कच्चे मॉडल Tmin को अकेले पूर्वानुमानक के रूप में उपयोग करने की उपयोगिता सीमित हो जाती है। एक व्यावहारिक, स्थल-विशिष्ट संकेतक के रूप में, जब मॉडलित $\Delta \leq$ लगभग 1.3 °C और पवन वेग $u \leq 2$ m s^{-1} एक साथ हों, तब उच्च पाला जोखिम को चिह्नित किया जाता है। ये सीमाएँ प्रारंभिक हैं, जो एक ही स्थल पर पाला-युक्त रातों से प्राप्त की गई हैं, और संवेदनशीलता व विशिष्टता को मात्रात्मक रूप से आँकने के लिए गैर-पाला नियंत्रणों तथा ROC/Youden विश्लेषण के साथ अंशांकन की आवश्यकता है। परिणाम जटिल उष्णकटिबंधीय उच्चभूमियों में प्रारंभिक

पाला-जोखिम संकेत के लिए एक सरल, प्रेक्षण-आधारित दृष्टिकोण का समर्थन करते हैं, साथ ही स्थिर रात्रिकालीन परिस्थितियों में मॉडल की सीमाओं को भी रेखांकित करते हैं।

ABSTRACT. Frost on the Dieng Plateau (Central Java, Indonesia) is examined using 10-min observations from Batur AWS and WRF-ARW hindcasts for eight events (05–10 August; 01–02 September 2023). We diagnose near-surface thermodynamics via dew-point depression ($\Delta = T - Td$) and assess two physics configurations. Across most nights, air approached saturation with $\Delta\text{min} \leq \sim 1–1.3$ °C, relative humidity ≈100%, and weak surface winds (often ≤2 m s^{-1}); Tmin typically occurred ~70 min after Δmin, indicating continued cooling once saturation is approached. One event departed from the Δ pattern, implying Δ is highly informative but not strictly necessary when micro-scale surface cooling diverges from shelter-level air. WRF reproduced the diurnal structure yet showed a systematic nighttime warm bias near minima, limiting the usefulness of raw model Tmin as a standalone predictor. As a pragmatic site-specific indicator, we flag high frost risk when modelled $\Delta \leq \sim 1.3$ °C coincides with $u \leq 2$ m s^{-1}. These thresholds are preliminary, derived from frost nights at a single site, and require calibration with non-frost controls and ROC/Youden analysis to quantify sensitivity and specificity. The results support a simple, observation-anchored approach to early frost-risk flagging in complex tropical highlands while highlighting model limitations under stable nocturnal conditions.

Key words – Frost prediction, Dieng plateau, WRF-ARW model, Meteorological conditions.

1. Introduction

The Dieng Plateau, recognized for its intricate topography and distinctive microclimate, is frequently subjected to the meteorological phenomenon of frost. Agricultural land use dominates this region, spanning 290 hectares and comprising 53% of the plateau's total area. Potato farms, which dominate this region, are most affected by frost, leading to crop withering and significant financial losses for farmers, ranging from IDR 800,000 to over 155 million (Pradana, *et al.*, 2018). Frost, being a critical environmental factor, not only limits the productivity and distribution of plants (Larcher W., 1981; Larcher and Bauer, 1981), but also serves as a major constraint for plant life (Sakai and Larcher, 1987). The occurrence of frost has significant implications for agriculture, ecology, and the local economy. The genesis of frost is a delicate balance of temperature, humidity, and various atmospheric conditions, and accurate prediction of these events can greatly reduce their negative impacts. This article probes the complexities of these meteorological factors, underscoring the importance of precise identification and prediction, particularly within the sensitive environmental context of the Dieng Plateau.

The likelihood of frost development on the Dieng Plateau extends beyond the mere aspect of altitude to include a range of specific meteorological conditions endemic to the region. Positioned at an elevation that is conducive to temperature inversions, the plateau is especially prone to frost, which is characterized by the deposition of ice crystals on surfaces under clear skies, stable winds, and low temperature regimes conditions that are routinely encountered in elevated terrains such as those found in the Dieng Plateau (Siswanto and Utomo, 2019). Based on these characteristics, the frost event on the Dieng Plateau is categorized as radiation frost. Radiation frosts are caused by radiant energy loss from the atmosphere, soil, and plant ecosystems on clear, no-wind nights (Kalma *et al.*, 1992; Ireland, 2005; Snyder and Melo-Abreu, 2005).

In recent years, the Weather Research and Forecasting (WRF) model and its Advanced Research (ARW) core have played a pivotal role in forecasting meteorological conditions. The WRF-ARW model stands out for its advanced physics schemes, high-resolution capabilities, and proficiency in simulating complex atmospheric phenomena, making it highly effective for predicting frost events. This model has not only been successfully employed in predicting frost events as demonstrated by Prabha and Hoogenboom (2008) but has also shown considerable utility in tropical regions, as evidenced by the work of Machado *et al.* (2018) and Bussoni *et al.* (2022).

Nonetheless, the task of forecasting frost events on the Dieng Plateau is challenging. The plateau's microclimatic variability, dictated by its topography, requires a model configuration that is sufficiently fine-tuned to grasp such heterogeneity. This article evaluates the WRF-ARW model's proficiency in simulating the essential meteorological conditions for frost formation and assesses its performance in a region where a slight inaccuracy can lead to errors in mitigation decision making.

The research commences with the identification of the meteorological conditions associated with eight incidents of frost on the Dieng Plateau during the period of August to September, 2023. Then, simulations of these frost events were performed using the WRF-ARW model. The evaluation focuses on the model's capability to capture and represent frost phenomena. For frost formation, meteorological conditions such as surface air temperature, dew point, relative humidity, and wind patterns are analyzed. The Dieng Plateau presents considerable variability in these parameters over minor

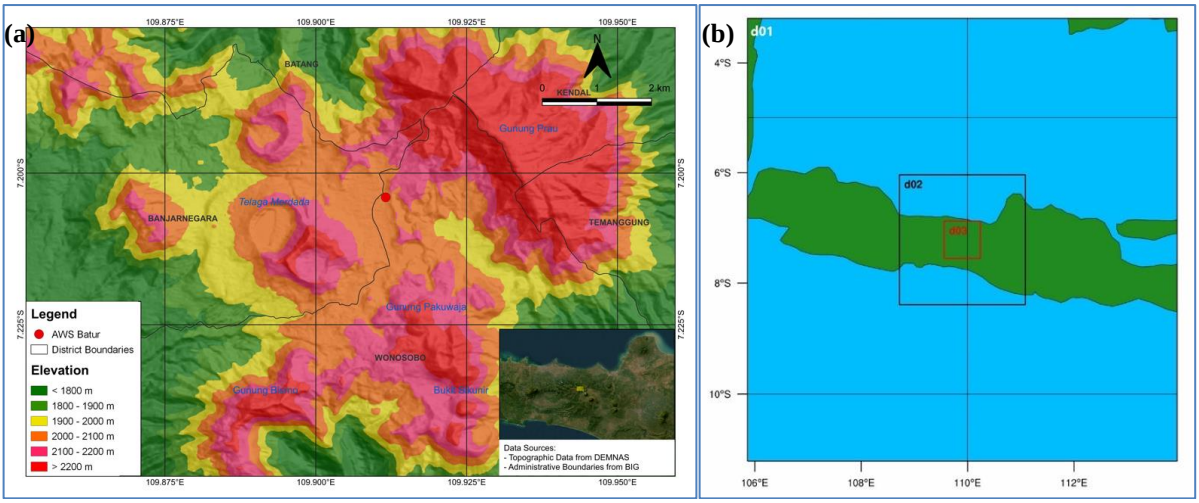

Figs. 1(a&b). Study area and model domains over the Dieng Plateau. (a) Orography (m) from DEMNAS with district boundaries from BIG; the Batur AWS is marked by a red dot and the inset shows the regional context. (b) WRF-ARW nested domains in Lambert Conformal Conic projection: d01 = 9 km, d02 = 3 km, d03 = 1 km. The innermost domain (d03) encloses the Dieng basin and the AWS site

distances, making frost prediction a sophisticated task. By examining the fidelity with which the WRF-ARW model reflects these conditions, the study not only benchmarks the model's precision but also identifies potential improvements.

The evaluation of the WRF-ARW model's accuracy in predicting frost occurrences on the Dieng Plateau is grounded in a review of essential literature, emphasizing the model's structural complexity (Skamarock, *et al.*, 2008) and criteria for frost occurrence (Snyder and Melo-Abreu, 2005). The research integrates perspectives on microclimate impacts on frost (Rossi *et al.*, 2022; Rozante *et al.*, 2019; and Huan *et al.*, 2021) and the influence of terrain on the accuracy of weather modeling (Jeworrek, *et al.*, 2021). The comparison of model simulations with real-world data aims to pinpoint enhancements to the model's predictive capabilities, thereby aiding the effective management of frost-related risks in the region. This investigative approach blends the intricacies of atmospheric modeling with the realities of meteorological forecasting, highlighting the necessity for high-resolution models in predicting frost, which is imperative for maintaining the Plateau's agricultural and economic stability.

2. Data and methodology

2.1. *Research location*

The study was undertaken on the Dieng Plateau, which lies within the administrative boundaries of Wonosobo and Banjarnegara Regencies in Central Java. From a geomorphological perspective, the plateau is characterized as a fluvial landscape, encircled by the volcanic terrains of Mount Prau, Mount Bismo, Mount Pakuwaja, and Mount Butak. The plateau's elevation ranges from 2,000 to 2,500 meters above sea level, with a general topographic gradient or surface runoff orientation toward the southwest. Fig. 1 shows the regional setting and the WRF nested domains (d01 = 9 km, d02 = 3 km, d03 = 1 km) enclosing the Dieng basin and the Batur AWS site.

2.2. *Datasets*

Primary data for analyzing the meteorological conditions that contribute to frost formation were obtained from the Batur Automatic Weather Station (AWS), positioned at a latitude of -7.20399 South and a longitude of 109.91158 East. The observational dataset from the AWS includes parameters such as surface air temperature (T), dew point temperature (Td), relative humidity (RH), and wind direction and speed (dddff). This suite of AWS data was not only pivotal for analyzing the conditions leading to frost but was also integral to the assessment of frost event simulations conducted using the Weather Research and Forecasting model with Advanced Research WRF core (WRF-ARW). The dataset spanned records from a total of eight frost occurrences, with six events occurring consecutively from 05 August to 10 August 2023, and two subsequent events on 01 September and 02 September 2023. The compilation of these frost event records was based on information reported by local communities.

For each 10-min AWS record we computed dew-point temperature Td from T and RH using the Magnus formula, $\gamma = ln\,(RH/100) + \frac{aT}{b+T}$ and $Td = \frac{b\gamma}{a-\gamma}$ with a=17.625 and b = 243.04°C. We then defined the dew-point depression Δ=T−Td as the primary diagnostic for near-surface saturation relevant to frost analysis.

For the simulation of frost episodes, Final Analysis (FNL) data, sourced from the National Center for Environmental Prediction, corresponding to the frost event dates, were utilized to establish initial and boundary conditions within the WRF-ARW version 4.4.1 model. This FNL dataset, characterized by a spatial resolution of 0.25° x 0.25°, is systematically updated at 6-hour intervals, thereby providing a robust framework for atmospheric model initialization and boundary condition specification.

2.3. *Procedures*

To ascertain the onset of frost, we meticulously examined ten-minute meteorological data recorded by AWS Batur, correlating frost reports with concurrent observations of temperature, dew point, relative humidity and dew point depression. This examination looked for discernible regularities that might be seen in the eight frost instances, allowing for the estimation of threshold values for these parameters indicative of imminent frost. Moreover, wind speed and direction were scrutinized due to their influence on thermal and moisture dispersion, with calm air conditions consistently preceding frost formation. We analysed the nighttime window 21:00–24:00 UTC for each frost night (05–10 Aug, 01–02 Sep 2023). Per night we derived: (*i*) the minimum 2-m air temperature T_{min} and its time; (*ii*) the minimum dew-point depression Δ_{min} and its time; (*iii*) the maximum relative humidity RH_{max}; (*iv*) 10-m wind statistics (median and minimum speed); and (*v*) the offset between T_{min} and Δ_{min} in minutes (positive when T_{min} occurred after Δ_{min}). Night-by-night values were summarised using medians across the eight events. We report a conservative necessary-condition threshold based on the largest Δ_{min} still associated with frost in our sample.

Subsequently, the simulation process in this study employed downscaling and two-way nesting procedures on Final Analysis (FNL) data within the Weather Research and Forecasting model with Advanced Research WRF core (WRF-ARW). This approach yielded data across three nested domains: a 9 km resolution for domain 1 (d01), a 3 km resolution for domain 2 (d02), and a 1 km resolution for domain 3 (d03), with a particular focus on domain 3 encompassing the Dieng Plateau. A 24-hour spin-up was executed to stabilize the model. The selection of parameterization schemes is pivotal in numerical modelling for simulating physical processes at unresolvable scales (Stensurd, 2007).

The simulation are case-study hindcast for 05–10 August and 01–02 September 2023. Model outputs were written hourly. We define the integration hour τ (equivalent to forecast lead time) as the elapsed time after initialization, i.e. τ= H+0, H+1, …, H+N. All results reported below use all hourly outputs after the 24-h spin-up within the study periods. All runs were conducted as independent cold starts (no cycling or FDDA/nudging), with lateral boundary conditions updated every 6 h from FNL.

Because frost forms under nocturnal radiative cooling, shortwave radiation choices primarily affect daytime evolution and cannot by themselves explain night time near-surface temperature errors. We therefore document, alongside shortwave/longwave radiation, the surface-layer formulation, PBL scheme under stable conditions, and the land-surface model, as these govern turbulent coupling, longwave cooling, and surface heat storage at night.

This study implements two distinct parameterization schemes: the Tropical Physics Suite (TPS) and the scheme developed by Bussoni *et al.* (2022), hereafter referred to as the 'Bussoni' scheme. These schemes were chosen for their efficacy in predicting frost, with the Bussoni parameterization noted for its effectiveness in Brazilian contexts. A key difference between the two lies in their approach to radiation modeling. The TPS employs the Rapid Radiative Transfer Model for GCM applications (RRTMG) for both shortwave and longwave radiation, as outlined by Iacono *et al.* (2008). In contrast, the Bussoni parameterization utilizes the Dudhia scheme for shortwave radiation (Dudhia, 1989) and the Rapid Radiative Transfer Model (RRTM) for longwave radiation (Mlawer, *et al.*, 1997). The selection of these radiation schemes is grounded in their pertinence to the radiative processes integral to frost formation.

The subsequent phase entails the pre-processing steps within the Weather Preprocessing System (WPS), which incorporates three primary procedures: geogrid.exe, for defining the model domains; ungrib.exe, for extracting meteorological data from input files; and metgrid.exe, for interpolating the extracted data onto the model grids. Following this, the numerical processing stage proceeds, utilizing the data prepared during the pre-processing phase. This stage involves real.exe, which initializes the model atmosphere and surfaces, and wrf.exe, which integrates the atmospheric flow forward in time.

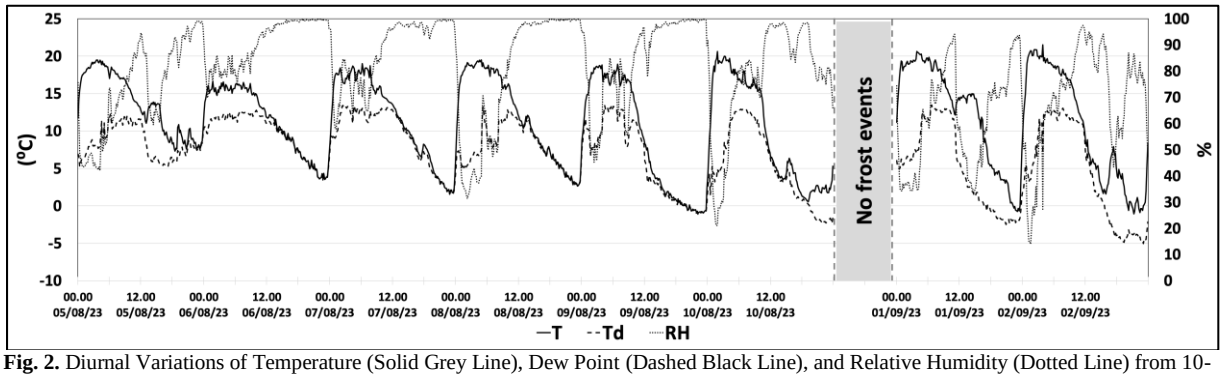

Fig. 2. Diurnal Variations of Temperature (Solid Grey Line), Dew Point (Dashed Black Line), and Relative Humidity (Dotted Line) from 10-Minute Intervals of AWS Batur Data in Relation to Frost Events during 05 – 10 August 2023 and 01 – 02 September 2023; UTC

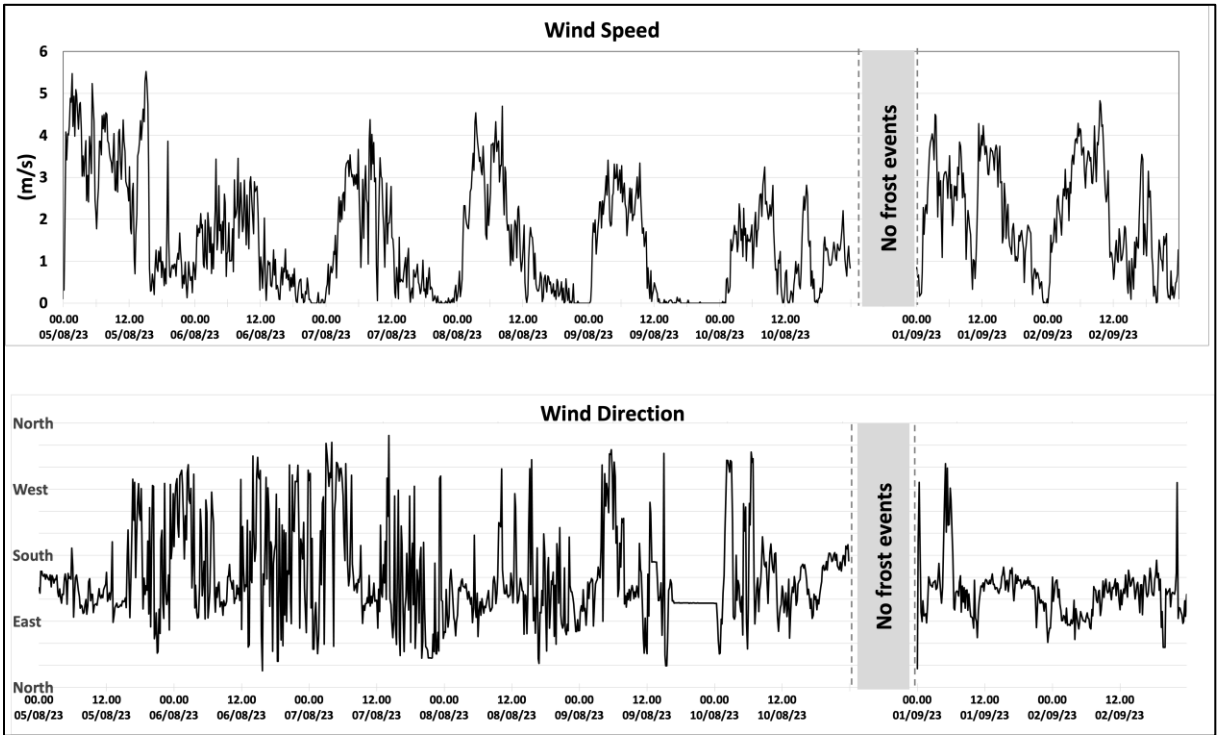

Fig. 3. Diurnal Variations in Wind Speed and Direction from 10-Minute Intervals of AWS Batur Data in Relation to Frost Events during 05 – 10 August 2023 and 01 – 02 September 2023; UTC.

Post-processing is conducted using ARW post, which translates the numerical results from the WRF-ARW model into output data files formatted as .dat and .ctl. Subsequently, the WRF-ARW model output files in the *.ctl format are compatible with the Grid Analysis and Display System (GrADS) for generating temporal representations of the model output.

The WRF-ARW model outputs, specifically surface air temperature (T), dew point temperature (Td), relative humidity (RH), wind speed (ff), and wind direction (ddd) at the Batur AWS location, are then juxtaposed with observational data from the Batur AWS. Model evaluation employs statistical parameters including the Root Mean Square Error (RMSE), Correlation coefficient (r), Mean Bias Error (MBE), Mean Absolute Error (MAE), and the Index of Agreement (d) to assess the model's performance.

3. Results and discussion

3.1. *Analysis of Meteorological Conditions Contributing to Frost Formation on the Dieng Plateau*

Across the eight frost nights, the composite diurnal cycle shows daytime warming and pronounced nocturnal cooling. During the frost window (≈ 04:00–07:00 LT /

TABLE 1

Parameterization configuration in running the model

	TROPICAL PHYSICS SUITE SCHEME (P1)			**BUSSONI SCHEME (P2)**		
Configuration	Domain 1 (d01)	Domain 2 (d02)	Domain 3 (d03)	Domain 1 (d01)	Domain 2 (d02)	Domain 3 (d03)
Spatial Resolution	9000	3000	1000	9000	3000	1000
Microphysical Scheme	WSM6	WSM6	WSM6	WSM6	WSM6	WSM6
Cumulus Scheme	-	-	-	-	-	-
PBL Scheme	YSU	YSU	YSU	YSU	YSU	YSU
Shortwave Radiation Scheme	RRTMG	RRTMG	RRTMG	Dudhia	Dudhia	Dudhia
Long Wave Radiation Scheme	RRTMG	RRTMG	RRTMG	RRTM	RRTM	RRTM
Surface Layer Scheme	Old MM5	Old MM5	Old MM5	MM5	MM5	MM5
Land Surface Scheme	Noah LSM	Noah LSM	Noah LSM	Noah LSM	Noah LSM	Noah LSM

TABLE 2

Nightly diagnostics on frost nights (21:00 – 24:00 UTC). Columns: **Date (night start),** *Tmin* **(°C), Time** *Tmin*, *Δmin* **(°C), Time** *Δmin*, **Offset [***Tmin−Δmin* **] (minutes), RH***max* **(%), Wind median (m s^{-1}), Wind min (m s^{-1}), % time** $u \leq 2$ **m s^{-1}, % time** $\Delta \leq 2$ **°C, % time** $\Delta \leq 1$ **°C, Wind-direction circular mean (°)**

Date (night start)	T_min (°C)	Time T_min (UTC)	Δ_min (°C)	Time Δ_min (UTC)	Offset (min)	RH_max (%)	Wind median (m s⁻¹)	Wind min (m s⁻¹)	% time u ≤ 2 m s⁻¹	% time Δ ≤ 2 °C	% time Δ ≤ 1 °C	Wind dir circular mean (°)
05/08/23	7.6	22:40	0.18	22:40	0	99.1	1.07	0.13	88.9	34.7	23.6	182.4
06/08/23	3.55	23:00	0.02	21:30	90	99.9	0.77	0	68.1	44.4	44.4	237.1
07/08/23	1.57	22:50	0.02	21:40	70	99.9	1.14	0	59.7	41.7	38.9	104
08/08/23	2.66	23:10	0.02	19:40	210	99.9	1.47	0	62.5	47.2	44.4	129
09/08/23	-0.96	22:10	0.02	20:10	120	99.9	0.04	0	94.4	41.7	40.3	115.1
10/08/23	0.57	19:10	0.28	19:00	10	98.6	1.26	0.64	96.7	10	6.7	172.3
01/09/23	-0.75	23:00	1.26	23:20	-20	93.7	1.73	0	58.3	12.5	0	108.2
02/09/23	-1.07	21:10	2.6	20:10	60	87.0	0.61	0	100	0	0	112.5

21:00–24:00 UTC), T approaches Td, and the dew-point depression $\Delta(t) = T - Td$ often falls below 1–2 °C for extended periods (Fig. 2). Relative humidity rises accordingly, frequently reaching ≥ 99%. These patterns indicate air close to saturation during the hours surrounding reported frost occurrence.

Wind speeds remain generally weak during the frost window, with median nocturnal $u \approx 1.1$ m s^{-1} and ~60–95% of nocturnal samples at $u \leq 2$ m s^{-1}, depending on the night (Fig. 3, Table 2). Wind direction exhibits large variability with circular means spanning ~100–240°, and no consistent directional preference emerges across events.

On individual nights (Fig. 4; Table 2), Δ_{min} ranged 0.02–1.26 °C for seven events and 2.6°C for one event (02 Sep 2023). The median Δ_{min} across all nights is 0.02 °C. The time offset between the saturation approach and the coldest air is positive: T_{min} typically occurs ~70 min after Δ_{min} (median), consistent with continued near-surface cooling after the dew-point depression reaches its minimum. Nights also feature near-freezing T_{min} (nightly median ≈ 1.6 °C), RH_{max} ≈ 99.9%, and weak winds (nightly median ≈ 1.1 m s^{-1})

Implication for a working indicator. In 7/8 nights, $\Delta_{min} \leq 1.3$ °C coincides with reported frost, suggesting $\Delta_{min} \lesssim 1$–1.3 °C as a useful rule-of-thumb for most events. The 02 September 2023 case (Δ_{min} = 2.6 °C, RH_{max} = 87%) departs from this pattern; it may reflect (i) a data/typing issue, (ii) a localized surface frost under relatively dry 2-m air, or (iii) representativeness differences. We therefore treat Δ_{min} as an informative but not necessary indicator, pending additional control nights and ROC analysis.

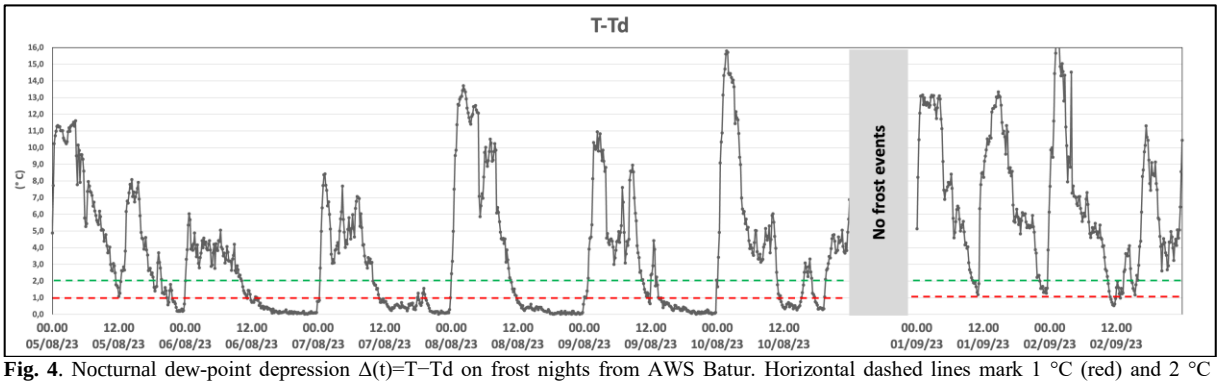

Fig. 4. Nocturnal dew-point depression Δ(t)=T−Td on frost nights from AWS Batur. Horizontal dashed lines mark 1 °C (red) and 2 °C (green) reference levels; UTC.

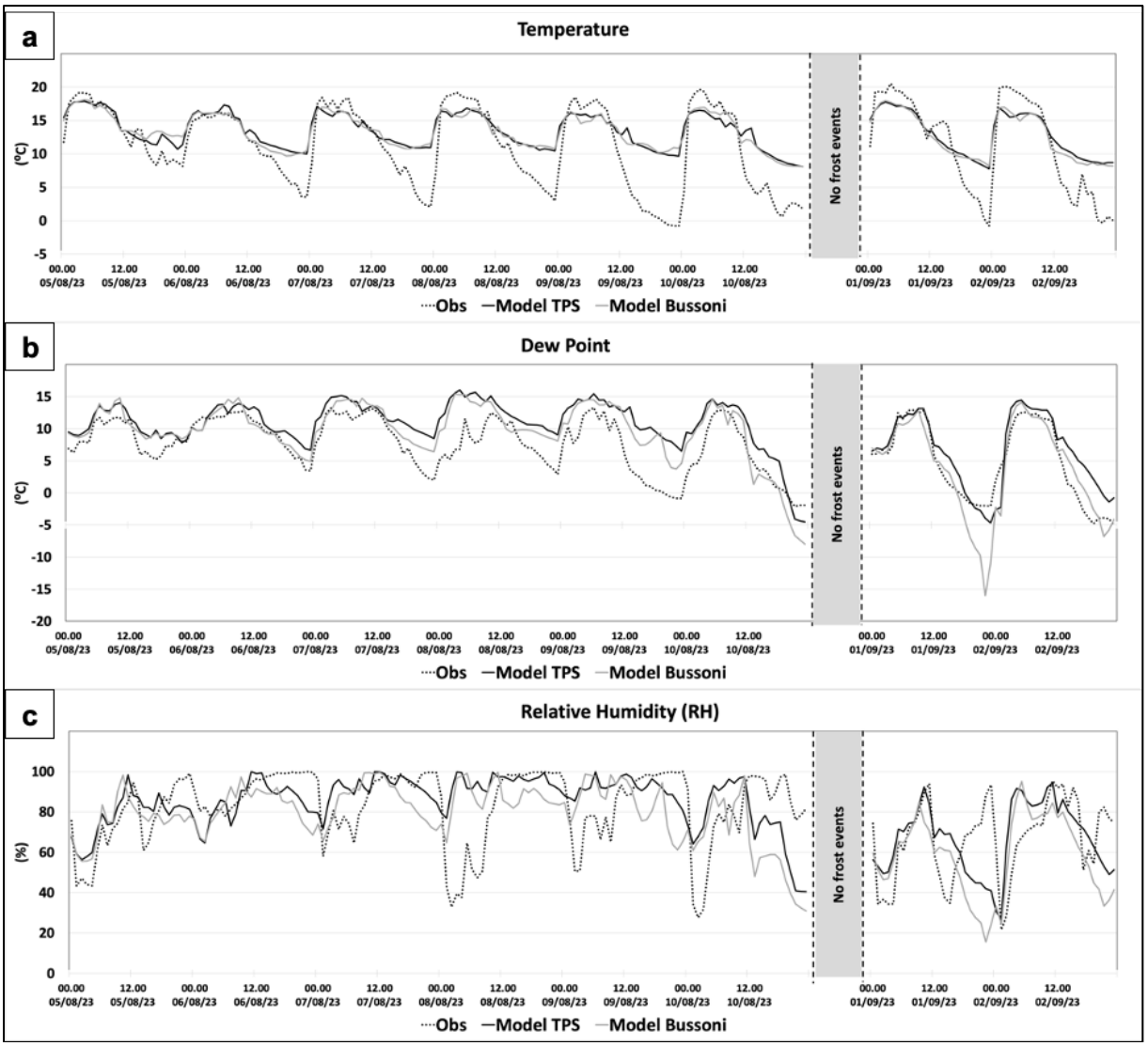

Figs. 5(a-c). Comparative Hourly Data of (a) Surface Air Temperature and (b) Dew Point Temperature in Degrees Celsius, and (c) Relative Humidity in Percentage; Based on Observations from AWS Batur (Dotted Black Line), Model Outputs from TPS (Thick Black Line) and Bussoni (Thick Grey Line) during 05 – 10 August 2023 and 01 – 02 September 2023; UTC

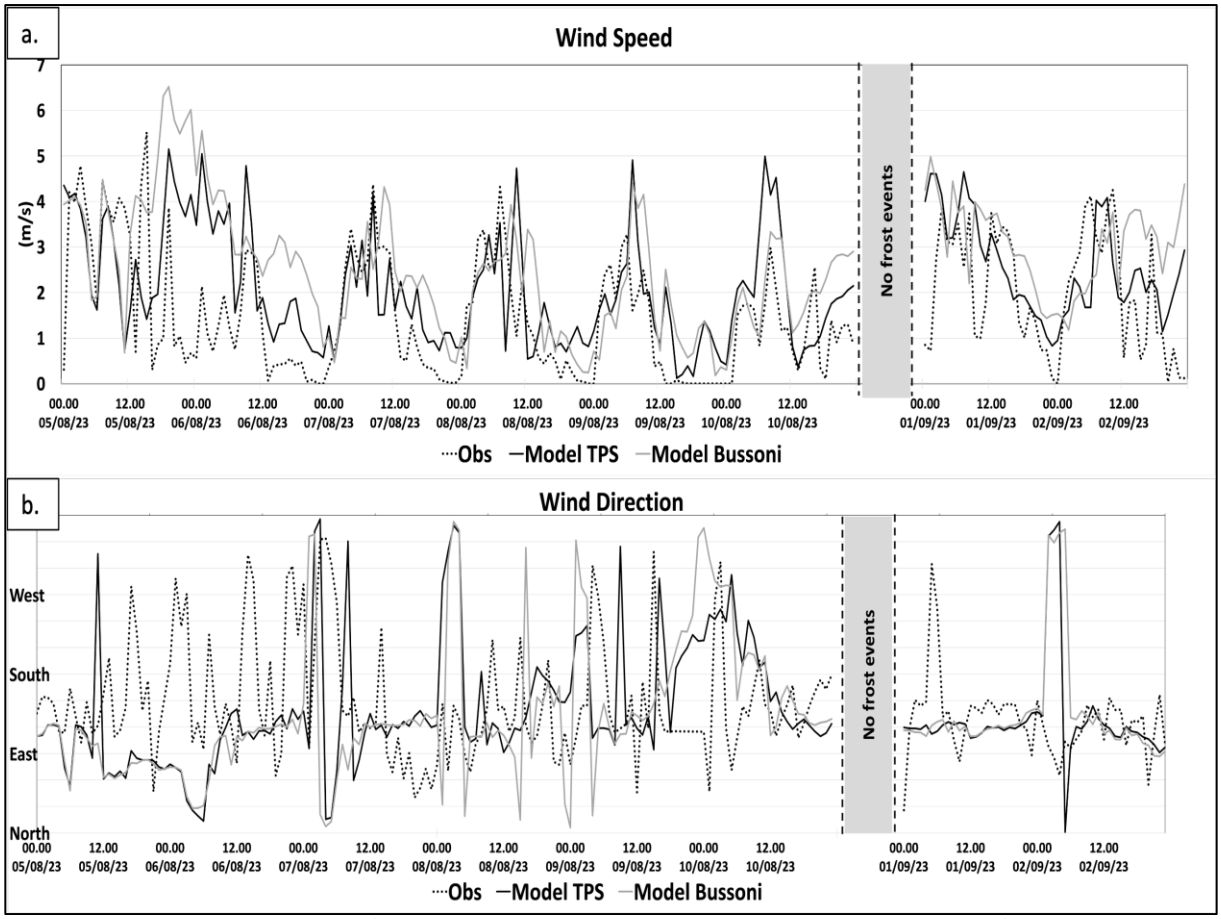

Figs. 6(a&b). Comparative Hourly data of (a) Wind Speed in m/s and (b) Wind Direction; Based on Observations from AWS Batur (Dotted Black Line), Model Outputs from TPS (Thick Black Line) and Bussoni (Thick Grey Line) during 05 – 10 August 2023 and 01 – 02 September 2023; UTC

3.2. *Evaluation of model performance in simulating frost events*

The diurnal patterns depicted in Fig. 5. Panel a reflect typical nocturnal lows and diurnal highs, with TPS and Bussoni models closely following observed trends but occasionally underestimating the cooling at night and peak daytime temperatures, suggesting potential inaccuracies in TPS's solar radiation parameterization. Dew point data, presented in Panel b, remains relatively stable, with night time values nearing air temperature, underscoring its role as a frost indicator. The models exhibit slight deviations from observed dew point data, hinting at variances in their moisture simulation. Panel c illustrates relative humidity trends, with saturation peaks aligning with the lowest temperature points, indicative of probable frost conditions; while both models replicate the general humidity cycles, they reveal differences at critical high humidity points essential for frost forecasting. Overall, the data and models present a coherent view of frost formation conditions, despite some model-data alignment discrepancies, particularly during nocturnal lows, essential for frost event simulation

In Fig. 6, the wind speed data (Panel a) does not exhibit a clear diurnal pattern, displaying variability and intermittent gusty conditions, with the Bussoni model showing a closer approximation to observed wind speeds than the TPS model. Discrepancies between both models and observed data highlight challenges in simulating local wind patterns and capturing short-term variations. The wind direction data (Panel b) shows significant directional shifts, with the TPS model reflecting some observed changes but with less precision, and the Bussoni model suggesting a more generalized or smoothed representation of wind patterns. These findings suggest that while both models provide valuable insights into wind behaviour over the Dieng Plateau, they have limitations in accurately reproducing the observed variability and transient features in wind patterns, which could be attributed to the complex influence of local topography on wind flow.

TABLE 3

Comparative Performance Metrics of TPS and Bussoni Models for Meteorological Parameters Over Dieng Plateau.

	RMSE		Correlation		MBE		MAE		d	
	TPS	**Bussoni**	**TPS**	**Bussoni**	**TPS**	**Bussoni**	**TPS**	**Bussoni**	**TPS**	**Bussoni**
T	4.42	4.37	0.91	0.91	2.09	1.99	3.42	3.32	0.77	0.78
Td	3.96	3.41	0.83	0.85	2.84	1.27	3.16	2.57	0.84	0.90
RH	19.61	23.03	0.43	0.30	2.36	-4.30	14.99	18.18	0.65	0.57
Ws	1.44	1.82	0.48	0.35	0.57	1.00	1.10	1.40	0.67	0.57
Wd	98.81	106.21	-0.12	-0.19	-5.85	-9.72	71.33	74.55	0.29	0.24

Table 3 shows the statistical analysis of the TPS and Bussoni models, using RMSE, Correlation, MBE, MAE, and Index of Agreement (d), reveals their predictive capabilities for meteorological parameters on the Dieng Plateau. The Bussoni model marginally outperforms the TPS in temperature (RMSE ~4.37 °C vs 4.42 °C; higher d) and dew point predictions (RMSE ~3.41 °C vs 3.96 °C; higher d). Conversely, the TPS model demonstrates a slight advantage in relative humidity and wind speed forecasting, reflected in lower RMSE and higher correlation figures. Both models, however, struggle with wind direction prediction, indicated by high RMSE and low correlation, highlighting the complexity of simulating wind patterns in mountainous terrain. Overall, the choice between models for operational forecasting should consider the parameter of focus, with the Bussoni model being slightly more favourable for temperature and dew point, and the TPS model for relative humidity and wind speed.

Given the nocturnal warm bias, minimum temperature from the model is not used directly for frost alerts. Instead, we leverage model fields that control nighttime cooling: dew-point depression $\Delta = T - Td$ and 10-m wind; and apply the AWS-derived necessary condition ($\Delta\text{min} \leq 1.3$°C under weak winds) as a categorical risk index. In practice, nights with modelled $\Delta \leq 1.3$°C concurrent with $u \leq 2$ m s^{-1} are flagged as high risk, consistent with the observed events. This indicator will be refined with additional non-frost control nights and ROC analysis in future work.

3.3. *Discussion*

Observations on the Dieng Plateau show that frost typically occurs under a recurrent nocturnal triad: near-saturation air ($\Delta = T - Td$ small), high RH, and weak winds. This is consistent with radiation-frost theory, in which clear, calm nights favour strong longwave cooling, stable boundary-layer formation, and surface decoupling. Prior work highlights the predictive value of a small T–Td spread and high RH (e.g., Perry, 1998; Snyder & Melo-Abreu, 2005; Gardner et al., 1991). In our eight-night sample, $\Delta\text{min} \leq$ ~1–1.3 °C co-occurs with reported frost in most cases, reinforcing Δ as a practical diagnostic of near-surface saturation. One night departs from this pattern, reminding us that Δmin is informative but not strictly necessary when micro-scale conditions (*e.g*., canopy/ground cooling) differ from shelter-level air. These findings corroborate earlier studies that identified small T–Td spreads and weak winds as critical precursors for radiation frost (Perry, 1998; Snyder & Melo-Abreu, 2005; Gardner et al., 1991). Specifically, the observed $\Delta\text{min} \leq$ 1–1.3 °C and RH ≈ 100% align with thresholds proposed by Rozante *et al*. (2019) and Rossi *et al*. (2022), who documented similar relationships between near-saturation conditions and frost occurrence in agricultural settings. The additional observation that T_{min} occurs ~70 minutes after Δmin further supports the role of continued radiative cooling, consistent with Pinto *et al*. (1977), who showed a marked discrepancy between shelter-level and ground-level temperatures during frost nights.

One event (02 September 2023) departed from the $\Delta\text{min} \leq 1.3$ °C criterion, which we interpret as either a localized surface frost under drier shelter air, or representativeness issues. This divergence illustrates the importance of including non-frost control nights in future work, but it does not contradict the broader radiation-frost framework, as similar exceptions have been noted in complex terrain studies (*e.g*., Rossi *et al*., 2022). The wind speeds observed to be below 2 m/s during frost episodes lend credence to the findings of Rozante *et al.* (2019) and Rossi *et al.* (2022), who recognized still air as essential for the radiative cooling necessary for significant temperature drops at the surface.

Although wind direction can influence local climatic conditions by transporting colder air masses, it appears to be of secondary importance to the thermal and moisture

dynamics identified as primary factors in frost development. The determination of a surface temperature threshold for frost prediction on the Dieng Plateau, specifically temperatures approaching or falling below 4 °C, aligns with the empirical findings of Rozante *et al.* (2019). This threshold is further substantiated by the research of Pinto *et al.* (1977), who noted a significant disparity, approximately 5.6 °C, between the air temperature recorded in a standard meteorological shelter and the ground-level temperature over grassy surfaces during frosty conditions. These insights underscore the critical importance of considering both shelter-level and ground-level temperatures in frost prediction models.

The performance of both TPS and Bussoni parameterization in simulating surface air temperature (T), dew point temperature (Td) and relative humidity (RH) is enhanced by their utilization of the WSM series microphysical schemes (Johnson, *et al.*, 2018) and the YSU planetary boundary layer scheme (Boadh, *et al.*, 2016), both of which have been empirically validated for accurate thermodynamic process representation. However, the slight differences in the configuration of the radiation and surface layer schemes between the two models may account for the nuanced differences in their performance. The TPS's use of RRTMG for both shortwave and longwave radiation schemes, which are known for their detailed spectral calculations (Iacono, *et al*., 2008), could explain its generally reliable temperature predictions.

On the other hand, the Bussoni model's implementation of the Dudhia shortwave scheme, coupled with the RRTM longwave scheme, is tailored for tropical regions and has shown promising results in capturing diurnal variations (Rashid *et al.*, 2022; Bussoni *et al.*, 2022). The warm bias of WRF during nocturnal minima mirrors findings by Jeworrek *et al*. (2021), who reported systematic errors in stable boundary-layer simulations over complex terrain. This consistency with prior work confirms that while the model captures diurnal structure, raw T_{min} should not be used directly for frost alerts without correction or supplementary indicators.

When discussing wind speed and direction, the spatial resolution plays a crucial role. Both models operate at 1 km resolution at domain 3 (d03), which is critical for capturing local topographical effects; however, the models' parameterizations might not fully resolve microscale dynamics that significantly impact wind patterns (Carvalho, *et al.*, 2012). The differences in surface layer schemes, with TPS using the older MM5 and Bussoni updating to newer MM5 in domain 3 (d03), may also influence the models' capacity to simulate surface-atmosphere interactions that affect wind prediction (Jiménez, *et al*., 2012).

The latest studies emphasize the importance of configuration settings in model performance, where even small changes can significantly impact simulations, particularly in complex terrain (Gómez-Navarro et al., 2015; Jeworrek *et al.*, 2021). While both models utilize the Noah land surface model, which has been shown to adequately simulate land-atmosphere energy exchanges (Chen and Dudhia, 2001a; Chen and Dudhia, 2001b), the interaction between this scheme and other model components is nontrivial and warrants further examination to understand its impact on wind modelling deficiencies.

Taken together, this study establishes a site-specific necessary condition for frost over Dieng: near-saturation nocturnal dew-point depression ($\Delta_{min} \leq 1.3$ °C) under weak winds, derived from high-frequency AWS observations of frost nights only. Because a curated set of non-frost nights is not yet available, we cannot quantify specificity or false-alarm rates at this stage. To complete the threshold framework, non-frost controls will be compiled from either (*i*) additional station nights in the same season without frost reports, or (*ii*) publicly available reanalysis (*e.g*., ERA5-Land) sampled over the Dieng grid for the same months, enabling frost vs non-frost distribution contrasts and ROC/Youden analysis for Δ_{min}, T_{min}, and wind. This will convert the present necessary condition into a calibrated, operational threshold with sensitivity and specificity.

4. Conclusions

Frost on the Dieng Plateau is characterized by near-saturation conditions and weak winds: in most events, the nocturnal dew-point depression was $\Delta min \leq$ ~1–1.3 °C, and Tmin occurred ~70 min after Δmin. While WRF reproduces the diurnal structure, a systematic nighttime warm bias limits the use of raw model Tmin as a standalone predictor. A practical risk flag for this site is therefore to classify nights as high-risk when modelled $\Delta \leq$ ~1.3 °C coincides with surface wind ≤ 2 m s^{-1}.

Overall, our analysis confirms the applicability of established radiation-frost mechanisms (small dew-point depression, high humidity, and calm winds) to tropical highlands, consistent with previous studies in other regions. At the same time, the identification of a $\Delta min \leq 1.3$ °C threshold under weak winds represents a novel site-specific diagnostic for Dieng Plateau, while the WRF nocturnal warm bias highlights the same limitations reported in prior modeling studies. These thresholds are preliminary and site-specific; they require calibration with non-frost controls and ROC/Youden analysis to quantify sensitivity and specificity before routine operational use.

Acknowledgements

The authors extend their sincere appreciation to the "Program Penelitian Unggulan 2023 dan Program Penelitian Mandiri 2024" at the State College of Meteorology, Climatology, and Geophysics, for their vital financial support and contributions throughout this research. Additionally, the authors would like to offer special thanks to the Indonesian Agency for Meteorological, Climatological, and Geophysics (BMKG) for granting access to the AWS Dieng dataset, which was crucial in facilitating this study.

Authors' contributions

Aries Kristianto: Conceived the study, led the overall research design, coordinated the meteorological analysis and wrote the first draft of the manuscript.
Imma R. Nugraheni and Deni Septiadi: contributed to the formulation of the research questions, meteorological interpretation, and critical revision of the text. (*email-imma.redha@stmkg.ac.id; deni.septiadi@stmkg.ac.id*).
Rista H. Virgianto: provided the climatological framework, contributed to the interpretation of the frost–climate relationships and assisted in refining the discussion. (*email-rhv24@cam.ac.uk*).
Hapsoro A. Nugroho: designed and implemented the modelling and computational setup, including WRF configuration and experimentation. (*email-hapsoro.agung@bmkg.go.id*).
Ita Soegiarto: contributed to data curation, literature review, preparation of supporting documentation and assisted in the organization, editing and formatting of the manuscript. (*email-itasoegiarto@gmail.com*).
Mawar J. Fadhilah and Tri Wahyudi: carried out data processing, quality control of AWS observations, preparation of figures and tables, and contributed to meteorological interpretation under the supervision of the lecturers. (*email-7mawarfadhilah12@gmail.com; tri.wahyudi@bmkg.go.id*).
Ravydo A. Jufri: assisted with engineering aspects of the modelling workflow, including preprocessing, running and troubleshooting of WRF simulations. (*email-ravydo30@gmail.com*).

All authors contributed to the interpretation of the results, reviewed the manuscript critically for important intellectual content and approved the final version for submission.

Disclaimer: The contents and views presented in this research article/paper are the views of the authors and do not necessarily reflect the views of the organizations they belong to.

References

Boadh, R., Satyanarayana, A., Khrisna, T. R., and Madala, S., 2016, "Sensitivity of PBL schemes of the WRF-ARW model in simulating the boundary layer flow parameters for its application to air pollution dispersión modeling over a tropical station", *Atmosfera*, 61-81.

Bussoni, C. V., Moreira, D. S., and Machado, J. P., 2022, "Evaluation of the WRF Model for the Application of a Frost Forecast Index in Southern Brazil (in Portugese with English summary)", *Revista Brasileira de Meteorologia*.

Carvalho, D., Rocha, A., Gómez-Gesteira, M., and Santos, C., 2012, "A sensitivity study of the WRF model in wind simulation for an area of high wind energy", *Environmental Modelling and Software*, 23-34.

Chen, F., and Dudhia, J., 2001a, "Coupling an Advanced Land Surface–Hydrology Model with the Penn State–NCAR MM5 Modeling System. Part I: Model Implementation and Sensitivity", *Monthly Weather Review*, 569-585.

Chen, F., and Dudhia, J., 2001b, "Coupling an advanced land surface-hydrology model with the Penn State-NCAR MM5 modeling system. Part II. Preliminary model validation", *Monthly Weather Review*, 587-604.

Dudhia, J., 1989, "Numerical study of convection observed during the winter monsoon experiment using a mesoscale two-dimensional model", *Journal of Atmospheric Science*, 3077-3107.

Gardner, W., McDonald, G., Ellis, S., Platt, M., and Flood, R., 1991, "A review of factors affecting minimum temperature reached on clear, windless nights", *Australian Journal of Agricultural Research*, 191-203.

Gómez-Navarro, J. J., Raible, C. C., and Dierer, S., 2015, "Sensitivity of the WRF model to PBL parametrisations and nesting techniques: evaluation of wind storms over complex terrain", *Geoscientific Model Development*, 3349–3363.

Huan, S., Yongguang, H., Yongzong, L., Jizhang, W., Qingmin, P., and Pingping, L., 2021, "A Review of Methods and Techniques for *Detecting Frost on Plant Surfaces*", *Agriculture*.

Iacono, M., Delamere, J., Mlawer, E., Shephard, M., Clough, S., and Collins, W., 2008, "Radiative forcing by long-lived greenhouse gases: Calculations with the AER radiative transfer models", *Journal of Geophysical Research*.

Ireland, W., 2005, "Frost and Crops: Frost Prediction and Plant Protection", Eastbourne, Self Published.

Jeworrek, J., West, G., and Stull, R., 2021, "WRF Precipitation Performance and Predictability for Systematically Varied Parameterizations over Complex Terrain", *American Meteorological Society*, 893-913.

Jiménez, P. A., Dudhia, J., González-Rouco, J. F., Navarro, J., Montávez, J. P., and García-Bustamante, E., 2012, "A Revised Scheme for the WRF Surface Layer Formulation", *Monthly Weather Review*, 898-918.

Johnson, A., Wang, X., Haghi, K., and Parsons, D., 2018, "Evaluation of Forecasts of a Convectively Generated Bore Using an Intensively Observed Case Study from PECAN", *American Meteorological Society*, 3097-3122.

Kalma, J., Laughlin, G., Caprio, J., and Hamer, P., 1992, "The Bioclimatology of Frost: Its Occurrence, Impact and Protection (Advances in Bioclimatology, 2)", *Berlin, Springer*.

Larcher, W., and Bauer, H., 1981, "Ecological significance of resistance to low temperature. In O. Lange, P. Nobel, C. Osmond, and H. Zielger", *Physiological plant ecology*, **1**, *Responses to the physical environment*, 403-438, Berlin, Springer.

Larcher, W., 1981, "Effects of low temperature stress and frost injury on plant productivity. In C. Johnson", *Physiological Processes Limiting Plant Productivity*, 253-269, Oxford, Butterworth-Heinemann.

Machado, J., Quadro, M., Cardoso, C., Araújo, C., Rodrigues, G., Costa, N., . . . de Paula, L., 2018, "Preliminary Evaluation of WRF

Physical Parameterizations for a Frost Event in Southern Brazil", *Meteorologica*, 3-23.

Mlawer, E., Taubman, S., Brown, P. D., Iacono, M. J., and Clough, S. A., 1997, "Radiative transfer for inhomogeneous atmospheres: RRTM, a validated correlated-k model for the longwave", *Journal of Geophysical Research*, 16663-16682.

Perry, K., 1998, "Basics of Frost and Freeze Protection for Horticultural Crops", *HortTechnology*, 10-15.

Pinto, H., Tarifa, J., Alfonsi, R., and Pedro, M., 1977, "Estimation of Frost Damage in Coffee Trees in the State of São Paulo, Brazil", *American Meteorological Society*.

Prabha, T., and Hoogenboom, G., 2008, "Evaluation of the Weather Research and Forecasting model for two frost events", *Computers and Electronics in Agriculture*, 234-247.

Pradana, A., Mardiana, A., Lestari, F. N., Sara, F. H., Afifah, S., and Nurjani, E., 2018, "Preliminary Assessment on Agricultural Impact due Frost (Embun Upas) Hazard in Dieng Highland, Central Java, Indonesia", *Agricultural Science*, 46-56.

Rashid, G. M., Hossain, M. T., Akhter, M. E., and Mallik, M., 2022, "Sensitivity of Radiation Schemes in the WRF-ARW Model to Predict Extreme Temperature Due to Heat Wave over Bangladesh", *IOSR Journal of Applied Physics*, 21-23.

Rossi, F., Facini, O., Loreti, S., Nardino, M., Georgiadis, T., and Zinoni, F., 2022, "Meteorological and micrometeorological applications to frost monitoring in northern Italy orchards", *Physics and Chemistry of the Earth*, 1077-1089.

Rozante, J., Gutierrez, E. R., Dias, P. L., Fernandes, A., Alvim, D. S., and Silva, V. M., 2019, "Development of an index for frost prediction: Technique and validation", *Meteorological Applications*, 1-12.

Sakai, A., and Larcher, W., 1987, "Low Temperature and Frost as Environmental Factors", Berlin, Springer.

Siswanto, and Utomo, J. B., 2019, "Suhu Dingin dan Embun Beku Saat Puncak Kemarau", *Klima: Layanan Multisektor BMKG Sebagai Bagian Pencapaian SDGs Aksi Iklim*, pp. 16-18.

Skamarock, W. C., Klemp, J. B., Dudhia, J., Gill, D. O., Barker, D. M., Duda, M. G., . . . Powers, J. G., 2008, "A Description of the Advanced Research WRF Version 3*"*, Boulder, Colorado, National Center for Atmospheric Research.

Snyder, R. L., and Melo-Abreu, J. P., 2005, "Frost Protection: fundamentals, practice and economics **1**", Rome, FAO.

Stensurd, D., 2007, "Parameterization Schemes: Keys to Understanding Numerical Weather Prediction Models", Cambridge, Cambridge University Press.